



# Mechanism for the water–gas shift reaction on monofunctional platinum and cause of catalyst deactivation

David W. Flaherty<sup>a,1</sup>, Wen-Yueh Yu<sup>a</sup>, Zachary D. Pozun<sup>b</sup>, Graeme Henkelman<sup>b</sup>, C. Buddie Mullins<sup>a,b,\*</sup>

<sup>a</sup> Department of Chemical Engineering, Texas Materials Institute, Center for Nano- and Molecular Science and Technology, Center for Electrochemistry, University of Texas at Austin, 1 University Station, CO400, Austin, TX 78712, United States

<sup>b</sup> Department of Chemistry and Biochemistry, Texas Materials Institute, Center for Nano- and Molecular Science and Technology, Center for Electrochemistry, University of Texas at Austin, 1 University Station, CO400, Austin, TX 78712, United States

## ARTICLE INFO

### Article history:

Received 17 May 2011

Revised 28 June 2011

Accepted 30 June 2011

Available online 4 August 2011

### Keywords:

Copper

Noble metal

Reforming

Model catalyst

Poisoning

Hydrogen

Reaction mechanism

## ABSTRACT

The behavior of monofunctional platinum, Pt(1 1 1), for the water–gas shift reaction has been investigated using experimental and theoretical methods. Kinetic and isotopic measurements performed from 525 to 675 K are consistent with an associative mechanism for the water–gas shift reaction in which carbon monoxide is oxidized by a hydroxyl group. The kinetically-relevant step consists of the unimolecular decomposition of an adsorbed carboxylate intermediate. The turnover frequency of Pt(1 1 1) is five times greater than that observed on Cu(1 1 1) under identical conditions (612 K, 26 Torr CO, 10 Torr H<sub>2</sub>O); however, Pt(1 1 1) loses activity over time due to the formation of carbonaceous deposits, a process not observed in similar studies of Cu(1 1 1). Our experimental and theoretical results suggest that CO dissociates via two pathways: the Boudouard reaction and through a COH intermediate. Nucleation of carbon at step-edges and subsequent oligomerization deactivate the catalyst. These results provide insight into the synergistic roles of noble metal clusters and active supports for the water–gas shift reaction.

© 2011 Elsevier Inc. All rights reserved.

## 1. Introduction

The water–gas shift reaction ( $\text{CO} + \text{H}_2\text{O} \rightarrow \text{CO}_2 + \text{H}_2$ ;  $\Delta H_{298\text{K}} = -40.6 \text{ kJ mol}^{-1}$ ) is important for the production of hydrogen for chemical processing and the elimination of CO contamination in feed streams for ammonia synthesis and fuel cells [1]. Due to the temperature dependence of the equilibrium constant, this reaction is conducted industrially in two stages: the first occurring at high temperatures over a chromium oxide-stabilized iron oxide catalyst that achieves fast turnover to moderate conversion and the second at low temperatures over zinc-promoted copper catalysts to reach complete conversion of CO [1,2]. However, the Cu–Zn catalysts traditionally utilized for the low-temperature water–gas shift reaction (WGSR) are pyrophoric, sensitive to poisons, and are unstable under conditions utilized for hydrocarbon reforming reactions [3]. Metal oxide-supported platinum clusters are already widely used for many reactions involving hydrocarbon conversion and are active for the WGSR [2–5]. Although platinum requires higher operating

temperatures, due to strong CO binding on the surface, platinum catalysts are inherently more stable and resistant to deactivation by heteroatoms, such as sulfur. Thus, platinum and platinum alloy catalysts are considered to be promising candidates for durable, high-activity water–gas shift catalysts [3,6,7].

Investigations of active noble metal-based catalysts (including platinum) for the WGSR have led to many important questions [3,5,8–13]. These questions concern the mechanism of the reaction, the role of the support, the identity of the active site, the relative activity of different metals, and the mechanism of deactivation. Mavrikakis, Dumesic, and coworkers conducted density function theory (DFT) calculations on Pt(1 1 1) in conjunction with experimental studies to probe the mechanism of alumina-supported platinum clusters for the WGSR and suggested that the reaction proceeded through a carboxylate (COOH) intermediate formed by direct oxidation of carbon monoxide by hydroxyl groups [5]. However, the redox mechanism, in which adsorbed water fully decomposes to form adsorbed atomic oxygen that subsequently oxidizes carbon monoxide [14], and active formate intermediates [8,14] have been reported on less inert oxide supports. Grenoble et al. demonstrated that the identity of the support had a significant effect on the turnover rate of the catalyst such that alumina-, silica-, and carbon-supported platinum catalysts exhibit relative activities of 90, 9, and 1, respectively [2]. More recently, Phatak et al. compared the activity of platinum catalysts supported on ceria and

\* Corresponding author at: Department of Chemical Engineering, Texas Materials Institute, Center for Nano- and Molecular Science and Technology, Center for Electrochemistry, University of Texas at Austin, 1 University Station, CO400, Austin, TX 78712, United States. Fax: +1 512 471 7060.

E-mail address: [mullins@che.utexas.edu](mailto:mullins@che.utexas.edu) (C.B. Mullins).

<sup>1</sup> Present address: Department of Chemical and Biomolecular Engineering, University of California at Berkeley, Berkeley, CA 94720, United States.

alumina supports and found that the turnover frequency (TOF) on the basis of exposed platinum atoms was 30 times greater for the ceria-based catalyst in comparison with that seen on alumina [4]. Turnover rate dependence on the identity of the catalyst support provides strong evidence for a bifunctional mechanism that is widely thought to include adsorption of CO on metal clusters and activation of water on the support [1,3]. Consequently, it has been postulated that the active site for the reaction may lie at the interface of these two regions [13,15]. One especially important issue is the comparative activity and stability of platinum-based water–gas shift catalysts with respect to catalysts based on other materials (e.g., copper); however, direct comparisons have only recently become available [16,17] due to numerous variations in the synthesis and testing procedures of earlier work [3,11]. Chorkendorff and coworkers recently compared turnover rates of 12 transition metals on both reducible and irreducible supports and found that the copper displayed the greatest TOF of the monofunctional catalysts (irreducible support); however, on reducible supports, platinum was by far the most active metal and copper among the least active [16]. Unfortunately, the metal dispersion on the reducible support could not be measured, making surface-averaged turnover rates impossible to determine. Finally, the mechanism by which supported cluster water–gas shift catalysts lose activity is unclear and in some cases has been attributed to the formation of inactive surface species, such as carbonates or formates, [18,19] or sintering and loss of metal surface area [19].

By decoupling the platinum catalyst from the support, it is possible to exclusively interrogate the catalytic activity of the metal component of these systems and thus determine the behavior of the monofunctional catalyst. This approach will be especially important in the design and testing of novel alloy systems (e.g., near surface alloys or bimetallics) in which an unsupported system will present the lowest level of complexity. Investigations of molecular transformations on single-crystal metals operating at technically relevant conditions have provided valuable, fundamental insights, which have aided in the understanding and design of catalysts for many important chemical reactions [20–24]. Relevant to the work reported here, Campbell et al. showed that kinetic parameters of the water–gas shift reaction on clean and modified Cu(1 1 1) and Cu(1 1 0) single-crystal surfaces closely matched those of technical catalysts and allowed the investigators to draw several important conclusions regarding the role of promoters such as Zn and Cs [25–27]. Successful study of these simple systems has enabled the study of more complicated model catalysts consisting of metal oxide-supported nanoparticles that mimic the activity and structure of industrial catalysts [28,29]. Rodriguez and coworkers have conducted a number of studies of the water–gas shift reaction over model catalysts comprised of gold [30–33], copper [30–33], and most recently platinum [30] nanoparticles dispersed on metal-oxide single crystal supports or inverse model catalysts created by the deposition of a metal oxide atop of a low-index plane of a metal single-crystal [9,34,35]. Interestingly, when nearly equivalent samples were created by deposition of identical atomic surface densities of platinum, copper, and gold (0.15 ML) onto ceria-modified TiO<sub>2</sub>(1 1 0), the platinum clusters were determined to be 25–50% more active than copper clusters, and ~180% more active than gold clusters [30]. However, observations by scanning tunneling microscopy (STM) clearly demonstrate that all three samples undergo noticeable morphological changes during the reaction period due to sintering [30]. Therefore, it is difficult to directly compare the activity of the three metals.

In this paper, we investigate the intrinsic catalytic behavior of the Pt(1 1 1) surface for the water–gas shift reaction at relevant pressures and temperatures. Alone and unsupported, Pt(1 1 1) catalyzes the water–gas shift reaction with an activation energy significantly greater than that of bifunctional catalysts. Kinetic

isotope effects (KIE) measured using H<sub>2</sub>O and D<sub>2</sub>O and the dependence of the rate on the pressure of the reactants suggest that the decomposition of a carboxylate intermediate [5] is the sole kinetically-relevant step under the conditions used here. Under identical conditions, the turnover rate for water–gas shift on the clean Pt(1 1 1) surface is ~five times greater than that of Cu(1 1 1) [25]; however, the rate on Pt(1 1 1) gradually decreases with time. CO dissociation occurs during the reaction, *via* the Boudouard reaction and also through a COH intermediate, and generates inactive carbon at the most reactive surface sites and diminishes the activity of the catalyst. These findings suggest that Pt-based WGS catalysts [2–5] can lose activity due to processes unrelated to sintering or carbonate formation, and technical catalysts may be negatively affected by similar carbonaceous deposits.

## 2. Methods

### 2.1. Experimental

Our experiments investigating the water–gas shift reaction on Pt(1 1 1) were conducted employing an ultrahigh vacuum (UHV) molecular beam surface scattering apparatus with a base pressure less than  $1 \times 10^{-10}$  Torr equipped with a high-pressure cell (HPC), which has been previously described in detail [36,37]. Briefly, the apparatus contains an Auger electron spectrometer (AES, Physical Electronics 10-500), a quadrupole mass spectrometer (QMS, Extrel C-50), a Fourier transform infrared spectrometer (FTIR, Bruker Tensor 27) combined with a mercury–cadmium–telluride detector (MCT, Infrared Associates) for reflection absorption infrared spectroscopy (RAIRS), as well as nozzles and apertures for generating two separate molecular beams that are used in conjunction with the QMS to conduct reactive molecular beam scattering (RMBS) as well as temperature-programmed desorption (TPD). Additionally, the chamber contains an Ar ion sputter gun for sample cleaning. The circular Pt(1 1 1) single crystal (MaTeck, 13 mm diameter x 1 mm thick) is spot-welded to a continuous loop of 1 mm diameter tantalum wire and mounted such that the sample temperature can be controlled by thermal contact, with a liquid nitrogen reservoir, and resistive heating over the range 77–1400 K as measured by a type-K thermocouple spot-welded to the top edge of the sample. The absolute temperature ( $\pm 2$  K) is verified using the known multilayer desorption temperatures of several small molecules. The clean Pt(1 1 1) surface is prepared by alternating cycles of high temperature annealing in oxygen (1000 K,  $5 \times 10^{-5}$  Torr), in vacuum (1200 K,  $\sim 2 \times 10^{-6}$  Torr), and Ar ion sputtering. The clean surface has less than 2% residual carbon and oxygen contamination as estimated by AES.

The water–gas shift reaction was conducted at elevated pressures (15–55 Torr) by vertically translating the sample into the HPC ( $V = 28.1$  L), which was isolated from the molecular beam scattering chamber using a gate valve. Water (HPLC-grade H<sub>2</sub>O, Fisher-Scientific; >99% D atom pure D<sub>2</sub>O, Spectra) and carbon monoxide (99.998%, Matheson) were rapidly introduced into the reaction chamber after purification. Water was thoroughly degassed under vacuum before use. The purity of the carbon monoxide was increased by passing it through a cartridge filled with molecular sieve 4A at 423 K followed by condensation within a copper loop submerged in liquid nitrogen at 77 K. This treatment effectively removed metal carbonyls such that post-reaction analysis of the sample surface composition never displayed any species other than platinum, oxygen, and carbon. The water–gas shift reaction was studied under batch reactor conditions, and the composition of the gas-phase was determined by analysis employing gas chromatography. To investigate the dependence of the reaction rate on the partial pressures of CO and H<sub>2</sub>O as well as to determine the

activation energy, the rate of H<sub>2</sub> or CO<sub>2</sub> production was monitored for 20 min after heating the sample to the reaction temperature. The gas-phase was sampled every 5 min in the manner described by Campbell and Daube [25]. Briefly, ~350 mL of gas, 1.2% of the volume of the reactor, is withdrawn from the batch reactor into a 0.25-in. diameter stainless steel tube. One end of this tube leads to the gas sampling loop for the gas chromatograph (GC, HP 5890), which is incorporated on a standard 6-port valve. By opening a valve at the opposite end of the stainless steel tube, high-pressure (45 psi) N<sub>2</sub> or He enters and compresses the large volume gas sample into the much smaller (10 mL) GC sample loop. Turnover frequencies were calculated by dividing the number of H<sub>2</sub> or CO<sub>2</sub> molecules produced per second by the number of platinum atoms at the surface, Pt<sub>s</sub>, determined from the product of the exposed surface area of the Pt(1 1 1) sample (2.65 cm<sup>2</sup>) and the atomic density of the Pt(1 1 1) facet (1.50 × 10<sup>15</sup> atoms cm<sup>-2</sup>). The GC was equipped with a thermal conductivity detector (TCD) and a packed column (Carboxen-1000, 1/8 inch diameter, 15 foot length, Supelco), which efficiently separated H<sub>2</sub>, CO, and CO<sub>2</sub> at 423 K. Water was removed from the gas sample before entering the gas chromatograph by passing the aliquot through copper tubing that was submerged in an ethanol solid–liquid mixture (~159 K) generated using liquid nitrogen. Turnover frequencies for investigating the effect of temperature and reactant pressure were calculated from the rate of formation of H<sub>2</sub> using N<sub>2</sub> as a carrier gas to provide the greatest sensitivity (He was implemented in select experiments to detect CO<sub>2</sub> and possible side products such as CH<sub>4</sub>). We estimated that uncertainties for the turnover frequencies reported in this study are less than ±10% as determined by repeated measurements of the H<sub>2</sub> formation rate at standard conditions of 25 Torr CO, 15 Torr H<sub>2</sub>O, at 625 K.

## 2.2. Computational details

Calculations for the microkinetic steps of the WGS on Pt(1 1 1) were performed using the Vienna *ab initio* Simulation Package (VASP) implementation of DFT [38–41]. Core electrons were treated as pseudopotentials using the projector-augmented wave method [42,43]. Valence electrons were described using Kohn–Sham single-electron wave functions expanded in a plane wave basis set with an energy cutoff of 274 eV [44,45]. The exchange–correlation contribution to the total energy functional was determined using the PW91 generalized gradient approximation (GGA) functional [46–48]. For all slab calculations, the face-centered cubic Pt(1 1 1) surface was modeled using four layers with the bottom two layers frozen into their bulk lattice positions with a lattice constant of 3.985 Å and the top layers allowed to relax [49]. A vacuum of at least 8 Å was used to separate periodic images above all surfaces. Energy barriers were calculated using the climbing-image nudged elastic band method (NEB) [50,51]. To improve efficiency, some saddle point energies were converged using the dimer min-mode following method [52,53]. Spin polarization was tested and applied where it was found to be necessary.

The bare Pt(1 1 1) surface was modeled using nine atoms per layer. Both (1 0 0) and (1 1 1) microfacets were considered as steps using fifteen and twelve atoms per layer, respectively. The Brillouin zone was sampled using a 4 × 4 × 1 Monkhorst–Pack k-point mesh [54]. Brillouin zone integration was converged using the finite-temperature method of Methfessel and Paxton with a smearing width of 0.2 eV [55]. The reference energy of a single carbon atom in a graphene sheet was calculated using the two-atom primitive cell with a Monkhorst–Pack 12 × 12 × 1 k-point mesh used to sample the Brillouin zone. The PW91 equilibrium graphene lattice constant of 2.465 Å, as calculated by Feibelman, was used in constructing the graphene primitive cell [56].

## 3. Results and discussion

### 3.1. Activity and composition of the Pt(1 1 1) surface

Fig. 1 shows the rate of formation of H<sub>2</sub> due to the water–gas shift reaction as promoted by the Pt(1 1 1) surface at 625 K in a mixture of 25 Torr CO and 15 Torr H<sub>2</sub>O. During this period, the Pt(1 1 1) surface is able to produce H<sub>2</sub> and CO<sub>2</sub> (not shown) catalytically with thousands of turnovers per surface platinum atom, Pt<sub>s</sub>. Rates of H<sub>2</sub> and CO<sub>2</sub> formation (measured in separate experiments) are comparable; however, turnover frequencies for CO<sub>2</sub> are typically greater. No other products (such as methane) that have been reported to form over supported noble metal WGS catalysts are observed [3]. Therefore, in the presence of CO and H<sub>2</sub>O, the Pt(1 1 1) surface solely catalyzes the water–gas shift reaction. Although the approach to equilibrium is negligible (the conversion is less than 0.1%), there is a clear decrease in the rate of H<sub>2</sub> production over the 75-min reaction period. Campbell and Daube observed a small decrease in the initial WGS reaction rate over the Cu(1 1 1) surface; however, the cause was not apparent, and they calculated quasi-steady state reaction rates from measurements taken during the first 12 min of reaction [25]. Post-reaction analysis of Cu(1 1 1) and Cu(1 1 0) samples demonstrated only small carbon coverages,  $\Theta_C \sim 0.07$  ML, which were independent of the reaction conditions and affected the reaction rates by less than 6% [25,57]. In contrast, Auger electron spectroscopy of Pt(1 1 1) following the water–gas shift reaction reveals somewhat larger coverages ( $\Theta_C \sim 0.05$ –0.3 ML), which are dependent on the duration, temperature, and prevalent gas composition. We have observed that the accumulation of carbon on the platinum surface has a negative effect on the reaction rate. Due to the sensitivity of this experimental technique, it is clear that the turnover frequency (TOF) may decrease by as much as ~50% between the first 2000 turnovers per site. In the present study, the hydrogen concentration as a function of time is described well by a second-order fit to the data during the first 20 min of reaction. The TOF of the pristine Pt(1 1 1) surface (in the limit of zero carbon coverage) is then calculated by the rate of hydrogen formation at the first instant of reaction, at  $t = 0$  (an illustration of this calculation is contained within the [Supplemental Information, Fig. S1](#)). In-depth discussion and information concerning the accumulation of carbon and the impact on the reaction mechanism and catalyst activity are addressed later in this article.

The TOF for the WGS on clean Pt(1 1 1) was determined at 25 Torr CO and 15 Torr water (utilizing either H<sub>2</sub>O or D<sub>2</sub>O) over

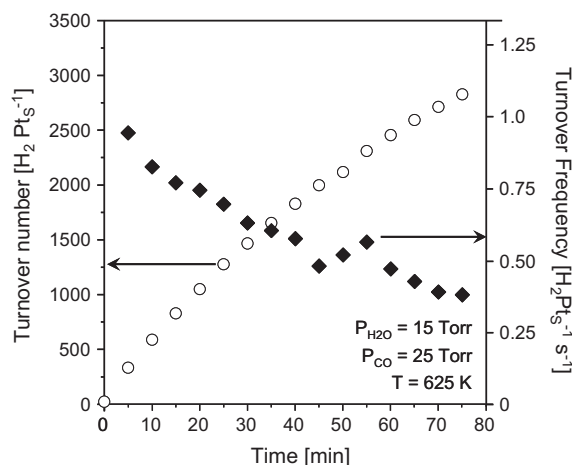


**Fig. 1.** Formation of H<sub>2</sub> due to the water–gas shift reaction with respect to time. The Pt(1 1 1) surface was rapidly heated to 625 K, and the gas-phase composition was determined by gas chromatography. The reactant gas composition was 25 Torr CO and 15 Torr H<sub>2</sub>O.

the temperature range 525–675 K. An Arrhenius plot of the turnover rates at these conditions is shown in Fig. 2. Over this temperature range, the values for the turnover frequency increase from 0.03 to 3.2 molecules  $\text{Pt}_5^{-1} \text{s}^{-1}$ . The activation energy,  $E_A$ , for the WGSR conducted with  $\text{H}_2\text{O}$  over Pt(1 1 1) was calculated to be  $96 \pm 3 \text{ kJ mol}^{-1}$ , and the  $E_A$  for the WGSR conducted with  $\text{D}_2\text{O}$  over Pt(1 1 1) was determined to be  $102 \pm 7 \text{ kJ mol}^{-1}$ . The experimental value of  $E_A$  for the reaction utilizing  $\text{H}_2\text{O}$  is similar to the value measured on Pt clusters on an inactive carbon support,  $106 \pm 6 \text{ kJ mol}^{-1}$ , at technically relevant pressures [2]. However, activation energies measured for WGSR over Pt on active supports are always lower by 20–30  $\text{kJ mol}^{-1}$  [2,4,5,13,16]. For example, Ribeiro et al. observed apparent activation energies of 68 and 75  $\text{kJ mol}^{-1}$  over alumina-supported and ceria-supported Pt clusters, respectively [4]. Additionally, Grenoble et al. observed that silica- and alumina-supported Pt clusters promoted the WGSR with apparent activation energies of 80 and 82  $\text{kJ mol}^{-1}$  [2]. Recent work by Mavrikakis et al. utilized DFT and microkinetic modeling to predict an apparent activation energy of 68  $\text{kJ mol}^{-1}$  over the Pt(1 1 1) surface, a value far smaller than our experimentally determined value, which was compared with a value of 71  $\text{kJ mol}^{-1}$  derived from experiments over Pt clusters supported on alumina [5]. However, it is noteworthy that alumina supports possess weak acidity, which may assist in activating water [58]. Indeed, Pt supported on alumina has a greater activity for WGSR and a lower activation energy in comparison with Pt supported on inert carbon [2]. Thus, some caution should be taken when correlating calculations regarding the Pt(1 1 1) surface and experiments performed on a clearly bifunctional catalyst.

A temperature-dependent kinetic isotope effect (KIE) is evident from the ratio of the rates measured using protonated and deuterated water,  $k_H/k_D$ , Fig. 2. The difference in  $E_A$  for WGSR with  $\text{D}_2\text{O}$  and  $\text{H}_2\text{O}$ ,  $\Delta E_{A,D-H} = E_{A,D} - E_{A,H}$ , is 6  $\text{kJ mol}^{-1}$ , and the ratio of the pre-exponentials,  $A_H/A_D$ , is about 0.8. Over the temperature range 575–675 K, the measured KIE,  $k_H/k_D$ , decreases from 2.3 to 1.9. Temperature-dependent kinetic isotope effects such as the one seen here are indicative of linear transition state structures [59,60]. The value of this KIE is larger than the value of  $\sim 1.3$  measured over ceria-supported Pt clusters at 523 K [8]. In both cases, the observation of a KIE is consistent with kinetically-relevant O–H/D bond rupture, which could occur during dissociation of water, hydroxyl groups, or carboxylate intermediates, or C–H/D bond rup-

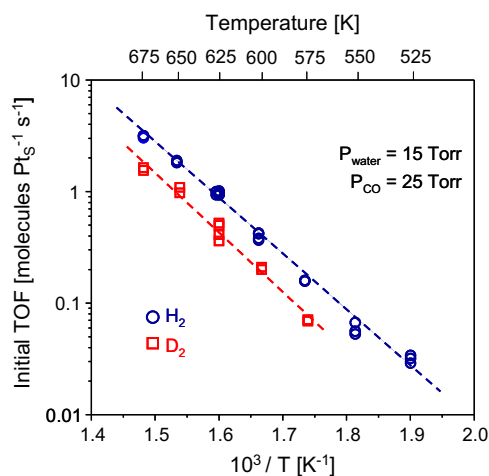


**Fig. 2.** Arrhenius plot of the formation rates of hydrogen and deuterium due to the water–gas shift reaction. The reactant gas composition was 25 Torr CO and 15 Torr water (either  $\text{H}_2\text{O}$  or  $\text{D}_2\text{O}$ ). Linear fits to the data for the rate of  $\text{H}_2$  (○) and  $\text{D}_2$  (□) production provide activation energies of 96 and 102  $\text{kJ mol}^{-1}$ , respectively.

**Table 1**

Comparison between the apparent activation energies and the absolute turnover frequencies (when available at equivalent conditions, expressed as molecules formed per surface metal atom,  $M_s$ , per second) for Pt(1 1 1) (this work), Cu(1 1 1) [25], Cu(1 1 0) [57], and Cu(1 0 0) [35] surfaces. The turnover frequencies for both systems were calculated under  $P_{\text{CO}} = 26 \text{ Torr}$  and  $P_{\text{H}_2\text{O}} = 10 \text{ Torr}$  at 612 K.

	$E_A$ ( $\text{kJ mol}^{-1}$ )	Turnover frequency (molecules $M_s^{-1} \text{s}^{-1}$ )
Pt(1 1 1)	96	$0.53 \pm 0.03$
Cu(1 1 1) [25]	71	0.10
Cu(1 0 0) [35]	64	–
Cu(1 1 0) [57]	42	–

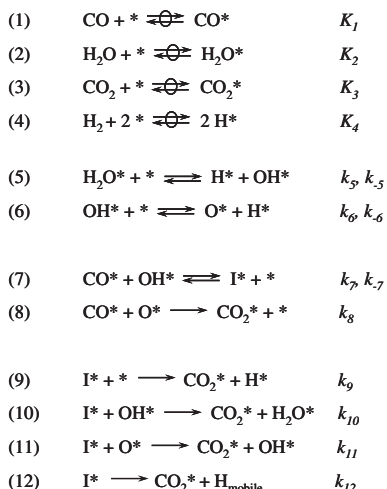
ture occurring during decomposition of a formate intermediate [8]. However, the fact that the rupture or formation of the isotopically labeled bond is kinetically-relevant is unambiguous. We will return to more discussion of the KIE in determining the mechanism of the reaction.

The apparent activation energy on the Pt(1 1 1) surface provides the first direct comparison with earlier studies of the WGSR on copper model catalysts, Cu(1 1 1) and Cu(1 1 0) [25–27]. Campbell and coworkers [25] measured the value of  $E_A$  on the Cu(1 1 1) surfaces to be 71  $\text{kJ mol}^{-1}$ , which is much lower than the barrier measured here on Pt(1 1 1) (96  $\text{kJ mol}^{-1}$ ). The Cu(1 0 0) [35] and Cu(1 1 0) [57] surfaces display lower values for  $E_A$ , only 64 and 42  $\text{kJ mol}^{-1}$ , respectively, presumably due to diminished barriers for water activation, the rate-controlling step [12], on these more open and coordinatively unsaturated surfaces [25–27,35,57]. In order to compare the close-packed (1 1 1) surfaces, the turnover frequency on the Pt(1 1 1) surface was determined under conditions identical to those utilized by Campbell and Daube during their study of WGSR on Cu(1 1 1) [25]. At 612 K, 26 Torr CO, 10 Torr  $\text{H}_2\text{O}$ , clean Pt(1 1 1) displayed a turnover frequency of  $0.53 \pm 0.03 \text{ H}_2 \text{ Pt}_5^{-1} \text{s}^{-1}$ , whereas Cu(1 1 1) was reported to have a turnover frequency of  $\sim 0.10 \text{ H}_2 \text{ Cu}_5^{-1} \text{s}^{-1}$  [25]. Therefore, at these conditions, Pt(1 1 1) surface has greater inherent activity for the water–gas shift reaction than Cu(1 1 1), see Table 1.<sup>2</sup>

However, the Pt(1 1 1) surface loses activity with time, which we attribute to accumulation of  $\sim 0.1$ – $0.15 \text{ ML}$  of carbon, and after  $\sim 20 \text{ min}$ , the turnover frequency is  $\sim 0.4 \text{ H}_2 \text{ Pt}_5^{-1} \text{s}^{-1}$ . Unfortunately, data reported on Cu(1 1 1) only extend to 12-min reaction times, so a comparison for greater times is not possible. However, the Cu(1 1 1) surface is reported to remain clean with less than  $\sim 0.07 \text{ ML}$  of contamination under all conditions investigated [25], so it appears that Cu(1 1 1) may be more chemically stable under reaction conditions than Pt(1 1 1).

Accurate information concerning the reaction mechanisms enables the design of more active catalysts tailored for specific applications; therefore, considerable efforts have been made to determine the mechanism of the water–gas shift reaction over various catalysts including supported Pt [1,2,4,5,8,11–14,16,19,61–64]. It has been proposed that noble metal catalysts promote the WGSR by either a redox or an associative mechanism; however, the details of the associative mechanism, including the identity of the active intermediates (e.g., carboxylate or formates), are still unresolved [3]. To elucidate the reaction mechanism on monofunctional Pt(1 1 1), we have considered a reaction network equivalent to that previously proposed by Mavrikakis and Dumesic [5], which contains elementary steps correlating to both the redox and associative mechanisms, Scheme 1. In the elementary steps and rate

<sup>2</sup> Low coordinate surface defects are expected to have an effect on the rates of WGSR on Pt and Cu. While we estimate that the defect concentrations are very small, they cannot be quantified.



**Scheme 1.** Reaction steps considered in determining the mechanism of the water-gas shift reaction on Pt(1 1 1). Unoccupied surface sites and the adsorbed species X are denoted by \* and X\*, respectively. The intermediate, I\*, represents the species HCOO and OCOH, the identity of which cannot be determined by rate behavior alone.

expressions, unoccupied surface sites and the adsorbed species X are denoted by \* and X\*, respectively. Note that the rate expressions make no assumptions concerning the structure of the intermediate I\*, which can represent carboxylate (OCOH) and formate (HCOO) species, the identity of which cannot be determined by rate behavior alone. Adsorption rates of the reactants (H<sub>2</sub>O and CO) and products (H<sub>2</sub> and CO<sub>2</sub>) are equal to the sticking coefficient (S, 10<sup>-4</sup>–1) multiplied by the flux to surface ~ 10<sup>6</sup> molecules Pt<sub>s</sub><sup>-1</sup> Torr<sup>-1</sup> determined from the kinetic theory of gases), whereas desorption rates can be calculated by the Polanyi–Wigner equation using pre-factors (10<sup>11</sup>–10<sup>13</sup> s<sup>-1</sup>) and known desorption energies on the Pt(1 1 1) surface [65–69]. At the temperatures and pressures employed here, it is apparent that the rates of adsorption and desorption are orders of magnitude greater than the overall forward rate of the reaction; therefore, the adsorption and desorption processes of the reactants and products, steps (1)–(4), are considered quasi-equilibrated. The TOF of the surface was measured over a range of CO and H<sub>2</sub>O pressures at 575 and 675 K. The dependence of the rate on CO and H<sub>2</sub>O, P<sub>CO</sub> and P<sub>H<sub>2</sub>O</sub>, at 575 K and 675 K, is shown in Figs. 3 and 4, respectively, and is extrapolated to the initial rate of reaction that occurs on the carbon-free surface (at t = 0, Fig. S1). In an attempt to derive an analytical expression for the reaction rate, we limit interpretation to Langmuir–Hinshelwood (L–H)-type rate expressions and assume the pseudo-steady state hypothesis (PSSH) such that the change in concentration of the surface intermediates is negligible during the course of the reaction [70]. We allow for changes in the surface coverage of intermediates and the kinetic relevance of different elementary steps.

Employing the elementary steps in Scheme 1 and the assumptions listed above, we derive an expression for the turnover frequency, which describes the experimental data for the WGSR on Pt(1 1 1):

$$r_{\text{WGSR}} = \frac{k_{\text{app}} \cdot P_{\text{CO}} \cdot P_{\text{H}_2\text{O}}}{\alpha^n} \quad (1)$$

where  $k_{\text{app}}$  denotes the apparent rate constant for the overall reactions, and the denominator  $\alpha$  represents the sum of the surface concentrations of all eight possible intermediates (unoccupied surface sites, \*, chemisorbed carbon monoxide, CO\*, etc.) that remains constant and equal to the number of adsorption sites at all times. The value of the exponent of  $\alpha$ , the variable  $n$ , is equal to the number

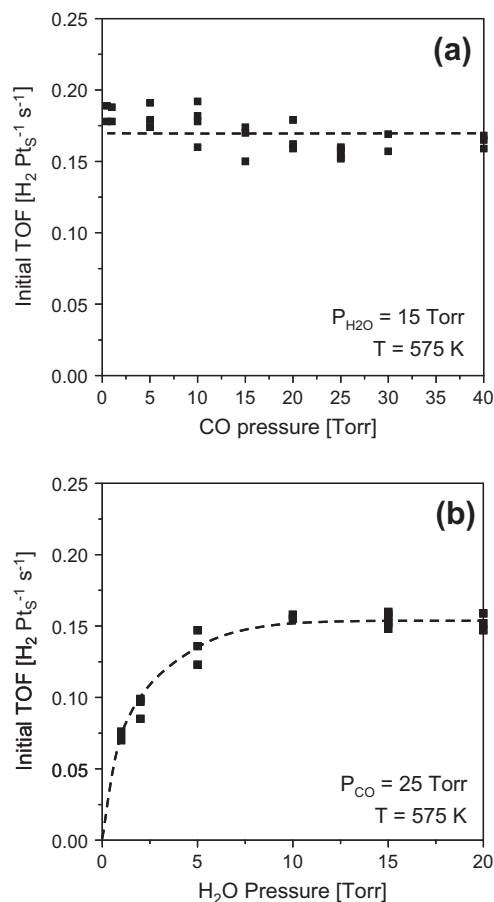


**Fig. 3.** Water-gas shift turnover frequency at 575 K. Dependence of rate on (a) the partial pressure of CO at 15 Torr H<sub>2</sub>O and (b) the partial pressure of H<sub>2</sub>O at 25 Torr CO.

of adsorption sites that participate in the kinetically-relevant elementary step. Under the conditions employed in this study, the rate dependence, outlined below, suggests that the most abundant surface intermediates (MASI) are limited to three possibilities:

$$\alpha = 1 + K_1 \cdot P_{\text{CO}} + \left( \frac{K_1 \cdot K_2 \cdot K_5 \cdot K_7 \cdot P_{\text{CO}} \cdot P_{\text{H}_2\text{O}}}{\sqrt{K_4 \cdot P_{\text{H}_2}}} \right) \quad (2)$$

where the three terms represent the concentrations of unoccupied sites, chemisorbed CO, and the intermediate, I\*, which at this point has an unknown structure. Additionally, we determine that the value of  $n$  is equal to one. A detailed derivation for Eqs. (1) and (2) is contained with the Supplemental Information.

As shown in Fig. 3a, the reaction rate has a near-zero-order dependence on  $P_{\text{CO}}$  over the pressure range of 0.5–40 Torr at 575 K. This is a consequence of a large value of the equilibrium constant for step (1),  $K_1$ , due to the strong binding energy of CO on the Pt(1 1 1) surface, which decreases with increasing coverage from ~140 to 110 kJ mol<sup>-1</sup> [67,68]; thus, in the presence of 40 Torr of pure CO, the Pt(1 1 1) surface remains covered with CO up to temperatures in excess of 700 K [71,72]. The rate dependence on  $P_{\text{H}_2\text{O}}$ , Fig. 3b, is best described as first-order when less than 5 Torr, above which it saturates at a TOF of ~0.15 H<sub>2</sub> Pt<sub>s</sub><sup>-1</sup> s<sup>-1</sup> and exhibits zero-order dependence. The observation of a zero-order dependence on  $P_{\text{H}_2\text{O}}$  is inconsistent with the kinetically-relevant dissociation of molecular water (5) or hydroxyl groups (6) and with CO oxidation by either hydroxyl groups (7) or chemisorbed oxygen (8) because any of these steps would lead to either a first-order or negative first-order dependence on  $P_{\text{H}_2\text{O}}$ . Note that regardless

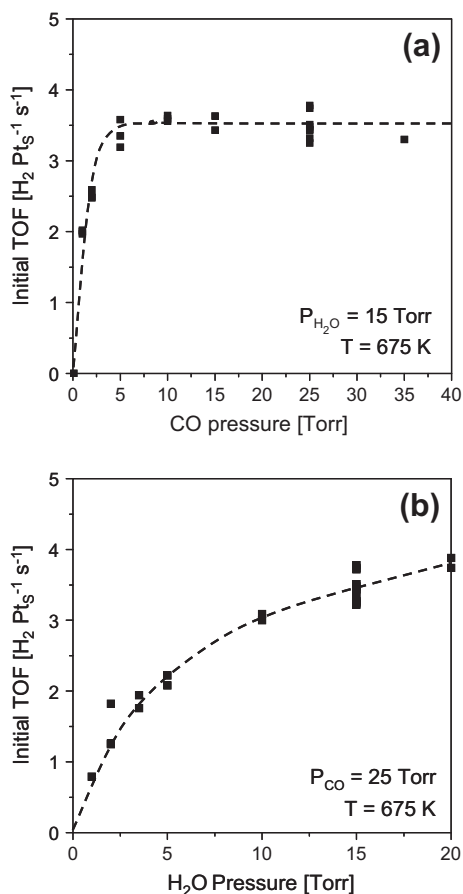


**Fig. 4.** Water–gas shift turnover frequency at 675 K. Dependence of rate on (a) the partial pressure of CO at 15 Torr  $\text{H}_2\text{O}$  and (b) the partial pressure of  $\text{H}_2\text{O}$  at 25 Torr CO.

of our choice of MASI ( $*$ ,  $\text{CO}^*$ , or  $\text{I}^*$ ), a zero-order dependence on both  $P_{\text{H}_2\text{O}}$  and  $P_{\text{CO}}$  is inconsistent, with steps (5)–(11) being kinetically-relevant. We are left with the conclusion that at 575 K, the rate-determining step involves the decomposition of the surface intermediate  $\text{I}^*$ , step (12), on a Pt(1 1 1) surface saturated with  $\text{I}^*$  (i.e.,  $\text{I}^*$  is the MASI). Consequently, this confirms that the associative water–gas shift mechanism dominates on monofunctional Pt(1 1 1), because  $\text{I}^*$  is formed by oxidation of  $\text{CO}^*$  with  $\text{OH}^*$  [5].

Similar conclusions are reached using observations at 675 K. As  $P_{\text{CO}}$  increases to 5 Torr, the reaction rate increases with a first-order dependence after which the rate becomes independent of  $P_{\text{CO}}$ , see Fig. 4a. This behavior is consistent with kinetically-relevant decomposition of  $\text{I}^*$  as the surface undergoes a transition from a predominantly empty surface,  $*$  as the MASI, to a surface covered by either  $\text{CO}^*$  or  $\text{I}^*$ . This demonstrates that steps (5)–(8) remain kinetically-irrelevant, as (5) and (6) could not explain the first-order dependence, and (7) and (8) would display an inverse dependence on  $P_{\text{CO}}$  as  $\text{CO}^*$  became the MASI at higher pressures [71,72]. Additionally, the previously mentioned KIE would not be observed if the rate-controlling step only involved C–O bond formation, as expressed in steps (7) and (8). Kinetically-relevant decomposition of  $\text{I}^*$ , steps (9)–(12), is consistent with the initial first-order dependence on  $P_{\text{CO}}$ ; however, assisted decomposition of  $\text{I}^*$  described in steps (9)–(11) would exhibit a negative first-order dependence on  $P_{\text{CO}}$  as the MASI transitioned from  $*$  to  $\text{CO}^*$  or  $\text{I}^*$ . Therefore, because we only observe a positive and zero-order dependency on  $P_{\text{CO}}$ , we rule out  $\text{I}^*$  decomposition as described in steps (9)–(11) and are once again left with step (12) as rate determining. Fig. 4b shows that increasing  $P_{\text{H}_2\text{O}}$  at 675 K increases the TOF initially with

a first-order dependence, for  $P_{\text{H}_2\text{O}}$  less than 5 Torr, and later with a sub-linear dependence, suggesting that the reaction rate becomes independent of  $P_{\text{H}_2\text{O}}$  at pressures greater than were experimentally accessible. Moreover, the dependence on  $P_{\text{H}_2\text{O}}$  matches the form of both steps (9) and (12) in the limit where the MASI is either  $*$  or  $\text{CO}^*$ ; however, the trend toward a zero-order dependence on  $P_{\text{H}_2\text{O}}$  in combination with the clear independence of the rate on  $P_{\text{CO}}$  is only consistent with step (12) on a surface covered by  $\text{CO}^*$  or  $\text{I}^*$ . Overall, this evidence indicates that within the conditions of this study, the rate dependence of the WGSR is consistent with kinetically-relevant single-site, unimolecular decomposition of  $\text{I}^*$ .

As indicated by the stoichiometry of step (12), the rate of liberation of atomic hydrogen in this elementary step appears to be independent of the concentration of adjacent unoccupied sites,  $*$ , or co-reactants,  $\text{OH}^*$  or  $\text{O}^*$ . The lack of a specific “landing site” for the hydrogen atom implies an early transition state that has no knowledge of the final configuration of the products. Additionally, the hydrogen atom may be highly mobile and able to access unoccupied sites or co-reactants over a distance of several lattice positions which is consistent with our assumption of quasi-equilibrated adsorption–desorption of  $\text{H}_2$ .

Aspects of the structure of the active form of the intermediate,  $\text{I}^*$ , can be determined by inspection of the observed kinetic isotope effect. The KIE seen for  $\text{D}_2\text{O}$  and  $\text{H}_2\text{O}$  for WGSR over Pt(1 1 1) shows a clear temperature dependence, with a value of  $\Delta E_{\text{A,D-H}}$  of  $6 \text{ kJ mol}^{-1}$ , and a ratio of the pre-exponentials,  $A_{\text{H}}/A_{\text{D}}$ , of 0.8, both of which are indicative of linear transition state structures [59,60]. An early transition state, with a structure more like that of the reactant than the product, is consistent with our prediction of the single-site decomposition of  $\text{I}^*$ , which implies that the hydrogen atom has little knowledge of its destination following O–H/D scission. However, the measured value of  $\Delta E_{\text{A,H-D}}$  is comparable to differences in the zero-point energies of O–H/D or C–H/D bonds,  $\sim 5\text{--}7 \text{ kJ mol}^{-1}$ , estimated from gas-phase vibrational spectroscopy, and suggests a nearly symmetric transition state (we note that uncertainty in values of  $\Delta E_{\text{A}}$  presented here are of the order  $\sim 5 \text{ kJ mol}^{-1}$ ). The ratio of the pre-exponentials,  $A_{\text{H}}/A_{\text{D}}$ , compares the difference in the entropy of the kinetically-relevant transition state between H/D isotopologues and offers a more reliable measure of the transition state structure [59]. Values of  $A_{\text{H}}/A_{\text{D}}$  in the approximate range of  $1/\sqrt{2}\text{--}\sqrt{2}$ , such as the value of 0.8 measured here, are associated with linear transition state structures, while ratios significantly greater than  $\sqrt{2}$ , such as 5 or more, are typical of bent transition states where the greater entropy of the H-isotopologue is indicative of the greater vibrational amplitude within a bent configuration [59]. Moreover, the H/D atom within a bent transition state possesses more residual motion than in a linear transition state, and therefore, the energy difference between the ground state and transition state for H and D isotopologues is similar, leading to temperature-independent kinetic isotope effects. We consider the differences in structure and surface coordination of the proposed reactive intermediates for the WGSR including formate,  $\text{HCOO}^*$ , and carboxylate,  $\text{OCOH}^*$ , and conclude that the reactive intermediate is carboxylate. The proposed model for the decomposition of  $\text{OCOH}^*$  occurs by O–H bond scission as the O–H bond stretches toward the Pt(1 1 1) surface [5] and is expected to be predominantly linear. On the other hand, the mechanism for C–H bond cleavage in formate necessitates a transition state dominated by bending modes because the C–H bond lies nearly perpendicular to the surface [8]. Therefore, decomposition of carboxylate,  $\text{OCOH}^*$ , by a linear transition state is most consistent with the observed kinetic isotope effects. Carboxylate intermediates have been proposed for the WGSR on both Pt(1 1 1) and Cu(1 1 1) surfaces,[5,12] and very recent work by Madon et al. suggests that on supported Cu catalysts, the WGSR largely proceeds via a carboxylate intermediate on a surface

primarily covered with inactive formate species [73]. Such a scheme is consistent with the rate dependence and kinetic isotope effects shown here, because the rate of formation of carboxylate and formate exhibits an identical dependence on  $P_{\text{CO}}$  and  $P_{\text{H}_2\text{O}}$ , step (7), although the equilibrium constants for each would differ to reflect their relative stabilities. Further studies utilizing in situ surface vibrational spectroscopy will be necessary to determine the identity of the MASI on the Pt(1 1 1) surface.

Considering that WGS proceeds by the associative mechanism with kinetically-relevant carboxylate dissociation on Pt(1 1 1), we briefly comment on this observation as to differences in  $E_A$  as measured on Pt clusters on different supports [2,4,5,13,16] and conclusions regarding the identity of the “active site” [13]. Whereas on the monofunctional Pt(1 1 1) surface, we have shown that the kinetic data for WGS are only consistent with unimolecular, single-site decomposition of carboxylate, other paths are certainly possible on bifunctional catalysts. As described by the pseudo-steady state hypothesis, all elementary steps preceding the kinetically-relevant step (or rate-controlling step) are considered to be chemically equilibrated [70]; thus, other reactive intermediates such as  $\text{OH}^*$  exist in concentrations determined by their Gibbs free energy of formation. These concentrations are low on Pt surfaces during the WGS [5,74,75]; however, reducible metal oxide supports can stabilize hydroxyl species and generate significant surface concentrations. Mavrikakis et al. identified several alternative elementary steps for the decomposition of  $\text{OCOH}^*$  that possess lower activation barriers, as compared to a unimolecular  $\text{OCOH}^*$  reaction, including  $\text{OH}^*$ -assisted decomposition of  $\text{OCOH}^*$  that occurs with an activation barrier of  $\sim 12 \text{ kJ mol}^{-1}$  (in this case, adsorption and activation of  $\text{H}_2\text{O}$  will become kinetically-relevant) [5]. Therefore, Pt clusters supported on reducible metal oxides ( $\text{TiO}_2$ ,  $\text{CeO}_2$ ) may display lower values of  $E_A$  due to significant flux through  $\text{OH}^*$ -assisted reactions pathways when hydroxyl species are loosely bound and readily available due to redox properties of the support [2,4,5,13,16]. Of course, in the absence of a support, e.g., on Pt(1 1 1), negligible surface concentrations of  $\text{OH}^*$  eliminate the possibility of  $\text{OH}^*$ -assisted  $\text{OCOH}^*$  decomposition. Recent proposals that the active site may lay at the Pt-support interface [13,15] may be rationalized considering the lower barrier of the  $\text{OCOH}^* + \text{OH}^*$  pathway, which would intuitively be promoted by the close proximity of  $\text{OCOH}^*$  and  $\text{OH}^*$  species adsorbed on the Pt and support, respectively.

### 3.2. Role of carbon during the WGS on Pt(1 1 1)

We have conducted the water–gas shift reaction over the Pt(1 1 1) surface for periods up to 180 min. From this data, it is clear that the rate of formation of  $\text{H}_2$  slows with time, as indicated for shorter periods in Fig. 1. During this period less than 0.2% of the CO and  $\text{H}_2\text{O}$  are converted to  $\text{H}_2$  and  $\text{CO}_2$  such that the concentrations of the reactants and the products vary little during this period. Therefore, the change in reaction rate must be due to deactivation of the Pt(1 1 1) surface. Post-reaction analysis of the Pt(1 1 1) surface by Auger electron spectroscopy demonstrates that significant amounts of carbon accumulate during the WGS and mostly probably this represents a mechanism for the decrease in activity. Fig. 5 displays Auger spectra obtained as a function of time following WGS on Pt(1 1 1) with  $P_{\text{CO}} = 25 \text{ Torr}$  and  $P_{\text{H}_2\text{O}} = 15 \text{ Torr}$  at 575 K (under these conditions, the WGS occurs with an initial TOF of  $\sim 0.2$  on the clean surface). Inspection of the spectral line-shape in the region of the carbon (KLL) Auger transitions,  $\sim 273 \text{ eV}$ , indicates that the carbon resides in an amorphous or graphitic chemical state, as opposed to a carbidic state [36,76]. Hemminger et al. utilized scanning tunneling microscopy to directly observe the structure and morphology of carbonaceous deposits formed by ethylene decomposition on Pt(1 1 1) [77,78].

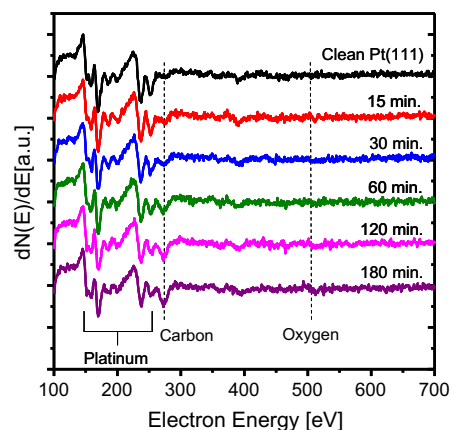


**Fig. 5.** Auger electron spectra of the Pt(1 1 1) surface following the water–gas shift reaction under  $P_{\text{CO}} = 25 \text{ Torr}$  and  $P_{\text{H}_2\text{O}} = 15 \text{ Torr}$  at 575 K. The sample was rapidly heated to 575 K in the reactant mixture. After the indicated times, the sample was held at 550 K while the chamber was quickly evacuated, followed by acquiring the Auger spectra at 550 K to prevent the accumulation of residual CO during analysis.

Notably, temperatures in excess of 800 K are typically necessary to transform amorphous carbon into a graphitic phase at coverages of  $\sim 0.20 \text{ ML}$  or less [77], although atomically thin graphite sheets have been produced at 700 K as carbon coverages approach saturation [78]. In this study, the absolute surface coverage of carbon is calibrated following the results of Koel et al. [79]. Utilizing low-energy electron diffraction, Auger electron spectroscopy, and temperature-programmed desorption, Koel et al. demonstrated (*via* a complete atomic balance on carbon and hydrogen) that formation of a saturation coverage of  $\text{C}_2\text{H}_4$  at 100 K (0.25 ML) followed by heating to 800 K leads to the formation of 0.22 ML of carbon on the Pt(1 1 1) surface [79]. Fig. 6 displays calculated carbon coverages as a function of reaction time for experiments at  $P_{\text{CO}} = 25 \text{ Torr}$  and  $P_{\text{H}_2\text{O}} = 15 \text{ Torr}$  at 575 K. Clearly, the carbon coverage increases monotonically with reaction time. We rule out the possibility of inactive formate species being responsible for the loss of activity [18,19] because the coverage of oxygen remains small,  $\theta_{\text{O}} < 0.03 \text{ ML}$ , and does not increase in proportion to carbon. Additionally, because the Pt(1 1 1) surface is unable to “sinter” or agglomerate, as suggested in the case of Pt clusters [19], it is evident that carbon accumulation is responsible for the loss of catalytic activity on the Pt(1 1 1) surface.

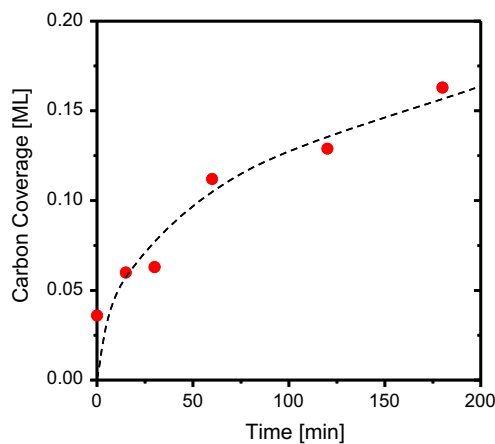


**Fig. 6.** Values of the carbon surface coverage determined *via* AES as a function of reaction time following the water–gas shift reaction under  $P_{\text{CO}} = 25 \text{ Torr}$  and  $P_{\text{H}_2\text{O}} = 15 \text{ Torr}$  at 575 K.

To confirm that carbon deposition occurs due to the WGSR and not due to the mere presence of impurities, additional experiments were performed in which the Pt(1 1 1) surface was exposed either to pure CO at 25 Torr or pure H<sub>2</sub>O at 15 Torr for 60 min at 575 K. The chamber was then evacuated and AES was utilized to determine the composition of the surface in vacuum. The results of these experiments are shown in Fig. 7 in comparison with the clean surface and with the surface following WGSR for 60 min at 575 K. Exposure to pure CO at 575 K results in carbon coverages of ~0.04 ML, and as expected, exposure to pure H<sub>2</sub>O at 575 K does not produce additional surface carbon either. On the other hand, simultaneous exposure of CO and H<sub>2</sub>O at 575 K induces a greater coverage of carbon, 0.08 ML, on the surface that is created as the surface produces H<sub>2</sub> and CO<sub>2</sub> via the water–gas shift reaction. However, the origin of the carbon is not immediately clear. Carbon could be present in stable formate and carbonate species which are known to form on supported platinum cluster catalysts during WGSR [3,62,80]. However, it is unlikely that this is the origin of the carbon observed in this study. First, the accompanying oxygen-to-carbon ratio would be expected to be two if formate species were present and three if carbonate species were present. Since the oxygen coverage is negligible, these species are certainly not present during the Auger measurement. Secondly, studies of formate decomposition over platinum surfaces have demonstrated that carbon is removed from the surface almost exclusively as CO<sub>2</sub> at temperatures less than 300 K [81,82], and carbonate desorbs from Cu–Pt alloys without leaving residual carbon [83]. Thus, in the event that these species do form during WGSR, their decomposition is not expected to be responsible for the carbon observed on the surface.

In order to determine the mechanism by which CO dissociates, we considered the elementary steps contained within the microkinetic model proposed by Mavrikakis et al. [5], and we simultaneously investigated the possibility of additional reaction pathways that could be responsible for the carbon deposition observed on the Pt(1 1 1) surface. The most straightforward possibility is CO splitting on the Pt(1 1 1) terrace. Fig. 8 illustrates that the minimum energy pathway for CO splitting contains a barrier of 3.27 eV and is endothermic by 1.89 eV. This barrier is not thermally accessible under experimental conditions, and equilibrium strongly favors CO over the formation of lone carbon atoms on the platinum surface. As expected, further DFT calculations demonstrate that the splitting of CO at steps has a slightly lower energetic barrier than on the Pt(1 1 1) terrace. For example, CO splitting at the (1 0 0) microfaceted steps on the Pt(1 1 1) surface (where CO binds in the fourfold hollow sites) has a barrier of 3.09 eV and is

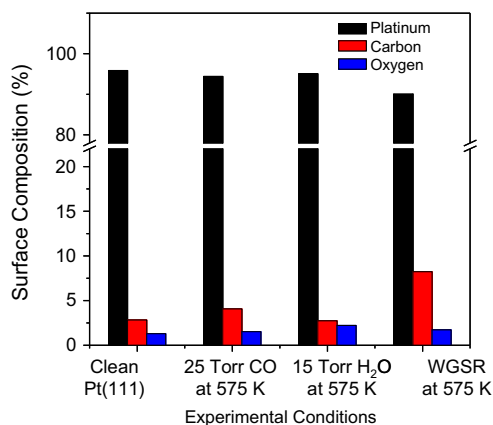


**Fig. 7.** Composition of the Pt(1 1 1) surface following exposure to the indicated gas mixtures at 575 K for a period of 60 min. The water–gas shift reaction was conducted at  $P_{\text{CO}} = 25$  Torr and  $P_{\text{H}_2\text{O}} = 15$  Torr at 575 K.

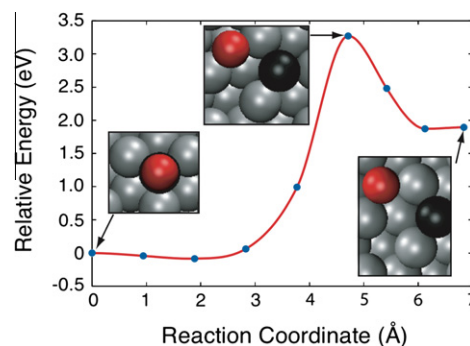


**Fig. 8.** The minimum energy pathway for CO splitting on the undefected Pt(1 1 1) surface as calculated by the NEB method. The colored spheres correspond to Pt atoms (silver), C atoms (black), and O atoms (red). (For interpretation of the references to color in this figure legend, the reader is referred to the web version of this article.)

endothermic by 2.26 eV. The barrier to CO splitting at the (1 1 1) microfaceted step is comparable, 3.05 eV. However, in comparison with both the (1 1 1) terrace and the (1 0 0) microfacet, carbon is much more stable at the (1 1 1) microfacet (the reaction enthalpy is lowered by ~1.2–1.5 eV, respectively). Therefore, due to the high energetic barrier for monomolecular splitting of CO, the carbon that is observed experimentally most likely originates from a different mechanism.

We have identified two potential pathways for the deposition of surface carbon by DFT. The first possibility is that the Boudouard mechanism may occur on the Pt(1 1 1) surface. Somorjai and coworkers have demonstrated that surface carbon can be generated via the Boudouard mechanism ( $2\text{CO} \rightarrow \text{C} + \text{CO}_2$ ) at CO pressures of 40 Torr over a Pt(1 1 1) surface at 673 K [66,71]. When identical experiments are performed over the Pt(5 5 7) surface, which contains a much higher density of step-edges, or over the Pt(1 0 0) surface, whose surface atoms have a lower coordination number, the temperature necessary for CO dissociation drops by more than 120 K [71]. In general, step-edges, kink sites, and low-coordination platinum atoms induce CO dissociation more readily. Using DFT, we have calculated a barrier of 2.38 eV for the Boudouard reaction occurring on the Pt(1 1 1) terrace, and the minimum energy path is shown in Fig. 9. This significant barrier is consistent with the experimental observation of only a slight increase in carbon to 0.04 ML following 60 min in 25 Torr of CO (no H<sub>2</sub>O) at 575 K, see Fig. 7. However, it is evident from Fig. 7 that the addition of H<sub>2</sub>O to the reactant mixture leads to greater carbon deposition,

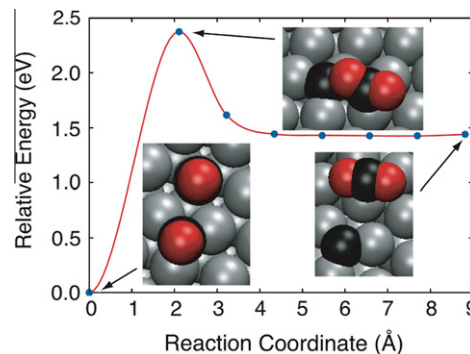


**Fig. 9.** The minimum energy path for the Boudouard reaction occurring on the Pt(1 1 1) terrace. A top site-bound and a hollow site-bound CO react to form C and CO<sub>2</sub>. The colored spheres correspond to Pt atoms (silver), C atoms (black), and O atoms (red). (For interpretation of the references to color in this figure legend, the reader is referred to the web version of this article.)

which implies an additional or alternative pathway involving adsorbed water or H<sub>2</sub>O-derived intermediates.

Using DFT, we have determined that the barrier for the dissociation of H<sub>2</sub>O is not directly affected by the presence of carbon atoms at neighboring sites, but hydroxyl groups will interact strongly with atomic carbon on the (1 1 1) terrace. In fact, as shown in Fig. 10, a single carbon atom will react with a hydroxyl to form a bound COH species with an energy barrier of 0.93 eV and  $\Delta E = -1.56$  eV. Once formed, this COH intermediate can access several exothermic pathways, which are summarized in Fig. 11. The COH may be deprotonated by the surface to form CO and H with a barrier of 0.88 eV and an energy difference between initial and final states of  $\Delta E = -0.23$  eV. Additionally, the COH intermediate may be deprotonated by a surface O to form CO and OH. This reaction occurs with a barrier of 0.29 eV and  $\Delta E = -0.38$  eV. Alternatively, COH may interact with a surface O atom to form the COOH intermediate considered by Mavrikakis et al. [5]. This pathway has a greater barrier of 0.98 eV; however, it is more exothermic than simple deprotonation reaction with  $\Delta E = -0.56$  eV. All of these reactions are thermally accessible under experimental conditions and ultimately form intermediates considered within the microkinetic model of Mavrikakis et al. [5]. Conversely, COH can decompose (COH dissociation into a hydroxyl group and surface carbon atom) with a barrier of 2.49 eV, which is comparable to the calculated barrier for the Boudouard reaction, 2.38 eV, and which can contribute to the increased rate of carbon deposition on the Pt(1 1 1) surface during the WGSR at 575 K for one hour. In summary, we speculate that both the Boudouard mechanism and decomposition of the COH intermediate contribute to the formation of carbon on the Pt(1 1 1) surface during the WGSR.

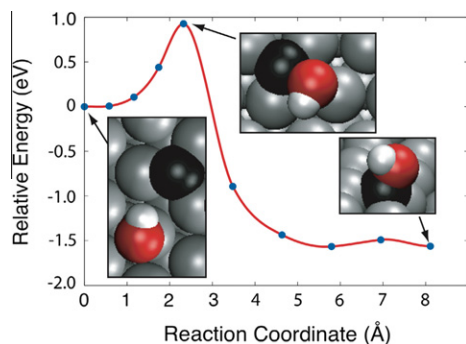


**Fig. 10.** The minimum energy path for a surface-bound hydroxyl and a carbon atom bound in a hollow site to form a COH intermediate. The colored spheres correspond to Pt atoms (silver), C atoms (black), O atoms (red), and H atoms (white). (For interpretation of the references to color in this figure legend, the reader is referred to the web version of this article.)

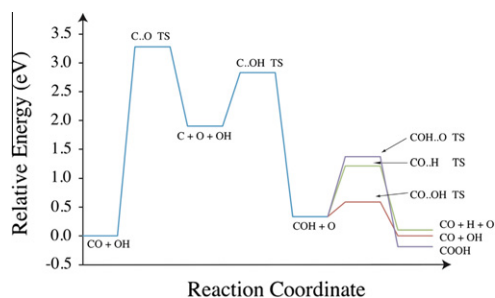


**Fig. 11.** The potential energy surface for CO splitting on Pt(1 1 1) followed by reaction with a surface hydroxyl to form COH followed by entry into the microkinetic model of Mavrikakis et al. [5].

DFT results indicate that the experimentally observed carbon accumulation on the surface is unlikely to consist of lone carbon atoms due to the unfavorable energetics and high reactivity of carbon atoms, as just discussed. If formed, the repulsion between lone carbon atoms in threefold hollows on the Pt(1 1 1) terrace will not allow them to be present in close proximity at concentrations as high as we have observed experimentally (0.2–0.3 ML following reactions at  $T = 625$  K). Fig. 12 shows the relative energy per carbon atom residing in threefold hollows on Pt(1 1 1) as a function of coverage in comparison with a single carbon atom bound in a graphene sheet. With increasing coverage, the relative energy per atom increases strongly until, at approximately two-thirds coverage, the surface will buckle. This comparison clearly indicates that equilibrium will strongly favor the formation of carbon–carbon bonds. Although, as shown in Fig. 12, a single carbon atom would be more stable in a graphene sheet by 0.64 eV, the nucleation of graphene is not favorable on the terrace. Chen et al. predict that the initial formation of carbon–carbon bonds is a kinetic limiting step in the growth of graphene on metal surfaces [84]. We calculate that carbon dimer formation at a step, to initiate graphene formation, is isoenergetic with two terrace carbon atoms. On the terrace, however, dimer formation is endothermic by  $0.5 \text{ eV} \cdot \text{atom}^{-1}$ . Graphene nucleation can be expected to occur, then, more readily on the step than on the terrace. Therefore, the (1 1 1) microfaceted step sites on the surface are the most likely potential location for the nucleation and anchoring of extended carbonaceous deposits containing C–C bonds. We expect that following nucleation at the (1 1 1) step, the carbonaceous deposits will continue to grow and extend further onto the (1 1 1) terrace, effectively blocking active sites and diminishing the catalytic activity of the surface.

The effect of low-coordination platinum sites (surface defects, step-edges, kink sites) was directly tested by comparing the water–gas shift activity of (1) the pristine, fully annealed and well-ordered Pt(1 1 1) surface and (2) the clean, yet highly defective Pt(1 1 1) surface generated by argon ion sputtering followed by annealing at 625 K in vacuum. Auger spectroscopy confirmed that each surface was initially free of carbon before the WGSR was initiated. After preparation, each sample was heated to 625 K in  $P_{\text{CO}} = 25$  Torr and  $P_{\text{H}_2\text{O}} = 15$  Torr, and the products were monitored with respect to time by gas chromatography. Each experiment was conducted three times, and the results were consistent. Fig. 13 displays the ensemble averaged turnover frequencies of both surfaces as a function of reaction time.

Three main points are evident from the data presented in Fig. 13. First, the initial TOF of the highly defective surface is 20–25% greater than that of the fully annealed and well-ordered Pt(1 1 1) surface. This result may be compared with related investigations of Campbell et al. on Cu(1 1 1) and Cu(1 1 0) surfaces

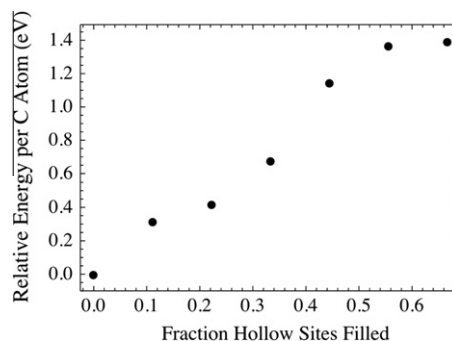


**Fig. 12.** The energy per surface-bound carbon atom on the Pt(1 1 1) terrace is plotted as a function of fractional surface coverage. The reference energy is the energy of a carbon atom in a single graphene sheet.

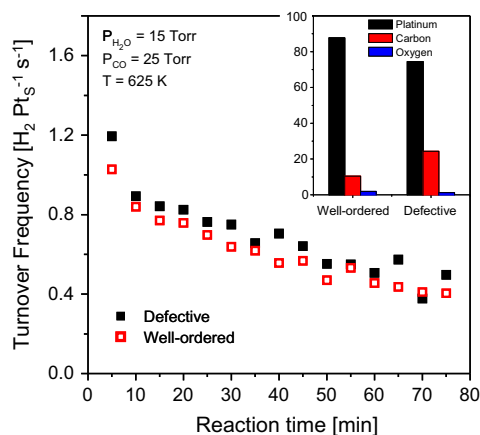


**Fig. 13.** Water–gas shift turnover frequencies as a function of reaction time for the highly defective Pt(1 1 1) surface and the well-ordered Pt(1 1 1) surface. The water–gas shift reaction was at  $P_{\text{CO}} = 25$  Torr and  $P_{\text{H}_2\text{O}} = 15$  Torr at 625 K.

where the Cu(1 1 0) possessed an inherent activity of  $\sim 2.5$ – $7$  times that of Cu(1 1 1) under a range of conditions [25,57]. The large difference in activity observed between Cu(1 1 1) and Cu(1 1 0) was attributed to the lower surface coordination number of Cu(1 1 0), which was thought to more rapidly catalyze dissociative adsorption of water, a rate-controlling step on that surface [57]. In the case of Pt(1 1 1), the decomposition of the carboxylate (OCOH) intermediate is rate controlling, and based on the differences in the initial TOF observed in Fig. 13, we expect that high concentrations of under-coordinated sites on the Pt(1 1 1) surface increase the rate of this step. Second, the highly defective surface loses activity more rapidly than the fully annealed and well-ordered Pt(1 1 1) surface. After 10–20 min of reaction, the TOF of the defective surface converges to that of the well-ordered surface such that whether the difference in the initial TOF is due to a change in the number of active sites or to an increase in the activity of the same sites, both surfaces demonstrate a nearly identical TOF after  $\sim 600$  turnovers. Third, recalling our proposed mechanism for deactivation, which predicts carbon nucleation at step-edges, we expect to observe an increased concentration of carbon on the defective surface due to the greater number of sites capable of stabilizing the carbon-chaining process. Indeed, post-reaction analysis of the surface composition reveals that the defective surface accumulates significantly larger amounts of carbon, 0.24 ML, while the well-ordered surface contains 0.10 ML carbon. Taken together, the activity and composition measurements suggest that highly reactive sites that are responsible for the majority of the catalytic activity of both Pt(1 1 1) surfaces are poisoned relatively quickly. The sample containing more reactive centers accumulates more carbon as a greater fraction of the surface sites are poisoned. Once carbon has poisoned the most reactive sites, the difference in concentration of which is responsible for the initial disparity in the reaction rates, the two surfaces ultimately approach similar values for the areal-averaged turnover frequency.

In our experience, the activity of the Pt(1 1 1) surface can be restored annealing the sample at  $T > 700$  K in low pressures of oxygen ( $\sim 10^{-5}$  Torr) or in higher pressures of water ( $\sim 10$  Torr). Following these treatments, Auger electron spectroscopy demonstrates that carbonaceous deposits on the surface have been removed, and the turnover frequency for the water–gas shift reaction returns to its original level. We conclude that the positive effect of co-feeding small amounts of oxygen during the WGSR over metal oxide-supported noble metal catalysts may be due in part to the removal of similar carbonaceous deposits on the metal clusters [18,85].

## 4. Conclusions

We have described the mechanism for the water–gas shift reaction on monofunctional platinum and the process responsible for the loss of activity over time. The dependence of the reaction rate on the pressure of CO and H<sub>2</sub>O at temperatures of 575 and 675 K is consistent with the unimolecular, single-site decomposition of an intermediate, I\*, formed from the oxidation of CO\* by OH\*, which occurs on a surface predominantly covered with CO\* or I\*. The observed temperature-dependent kinetic isotope effect suggests that I\* decomposes by a linear transition state, providing evidence that the active form of I\* is carboxylate (OCOH\*). Under identical reaction conditions, the monofunctional Pt(1 1 1) surface demonstrates an initial turnover frequency, which is five times greater than that observed on Cu(1 1 1). Loss of activity with time is attributed to CO dissociation via two pathways: the Boudouard reaction and the decomposition of a COH\* intermediate. Subsequent nucleation and oligomerization of carbon at step-edges preferentially deactivate the most active sites on Pt(1 1 1) surface. It is hoped that the results presented here will guide further studies to explore the improvement in platinum-based water–gas shift catalysts and the fundamental mechanisms by which this is achieved.

## Acknowledgments

C.B.M. acknowledges the Department of Energy (DE-FG02-04ER15587) and the Welch Foundation (F-1436) for their generous support. G.H. acknowledges the Welch Foundation (F-1601), the National Science Foundation (CHE-0645497), and the Texas Advanced Computing Center. D. W. F. thanks Mr. Robert Carr, Mr. Brett Loveless, and Mr. Rajamani Gounder for useful discussions.

## Appendix A. Supplementary material

Supplementary data associated with this article can be found, in the online version, at doi:10.1016/j.jcat.2011.06.024.

## References

- [1] C. Rhodes, G.J. Hutchings, A.M. Ward, *Catal. Today* 23 (1995) 43.
- [2] D.C. Grenoble, M.M. Estadt, D.F. Ollis, *J. Catal.* 67 (1981) 90.
- [3] C. Ratnasamy, J.P. Wagner, *Cat. Rev. – Sci. Eng.* 51 (2009) 325.
- [4] A.A. Gokhale, N. Koryabkina, S. Rai, J.L. Ratts, W. Ruettinger, R.J. Farrauto, G.E. Blau, W.N. Delgass, F.H. Ribeiro, *Catal. Today* 123 (2007) 224.
- [5] L.C. Grabow, A.A. Gokhale, S.T. Evans, J.A. Dumesic, M. Mavrikakis, *J. Phys. Chem. C* 112 (2008) 4608.
- [6] H. Iida, K. Yonezawa, M. Kosaka, A. Igarashi, *Catal. Commun.* 10 (2009) 627.
- [7] R. Radhakrishnan, R.R. Willigan, Z. Dardas, T.H. Vanderspurt, *Appl. Catal. B: Environ.* 66 (2006) 23.
- [8] G. Jacobs, S. Khalid, P.M. Patterson, D.E. Sparks, B.H. Davis, *Appl. Catal. A* 268 (2004) 255.
- [9] J.A. Rodriguez, S. Ma, P. Liu, J. Hrbek, J. Evans, M. Perez, *Science* 318 (2007) 1757.
- [10] Q. Fu, H. Saltsburg, M. Flytzani-Stephanopoulos, *Science* 301 (2003) 935.
- [11] R. Burch, *PCCP* 8 (2006) 5483.
- [12] A.A. Gokhale, J.A. Dumesic, M. Mavrikakis, *J. Am. Chem. Soc.* 130 (2008) 1402.
- [13] N.M. Schweitzer, J.A. Schaidle, O.K. Ezekoye, X.Q. Pan, S. Linic, L.T. Thompson, *J. Am. Chem. Soc.* 133 (2011) 2378.
- [14] K.G. Azzam, I.V. Babich, K. Seshan, L. Lefferts, *J. Catal.* 251 (2007) 153.
- [15] C.M. Kalamaras, S. Americanou, A.M. Efstathiou, *J. Catal.* 279 (2011) 287.
- [16] A. Boisen, T.V.W. Janssens, N. Schumacher, I. Chorkendorff, S. Dahl, *J. Mol. Catal. A: Chem.* 315 (2011) 163.
- [17] R. Radhakrishnan, R.R. Willigan, Z. Dardas, T.H. Vanderspurt, *AIChE J.* 52 (2006) 1888.
- [18] D. Pierre, W. Deng, M. Flytzani-Stephanopoulos, *Top. Catal.* 46 (2007) 363.
- [19] K.G. Azzam, I.V. Babich, K. Seshan, L. Lefferts, *J. Catal.* 251 (2007) 163.
- [20] D.W. Goodman, *Acc. Chem. Res.* 17 (1984) 194.
- [21] J.A. Rodriguez, D.W. Goodman, *Surf. Sci. Rep.* 14 (1991) 1.
- [22] C.V. Ovesen, P. Stoltze, J.K. Norskov, C.T. Campbell, *J. Catal.* 134 (1992) 445.
- [23] F. Zaera, A.J. Gellman, G.A. Somorjai, *Acc. Chem. Res.* 19 (1986) 24.
- [24] G.A. Somorjai, J.Y. Park, *Chem. Soc. Rev.* 37 (2008) 2155.
- [25] C.T. Campbell, K.A. Daube, *J. Catal.* 104 (1987) 109.
- [26] C.T. Campbell, B.E. Koel, K.A. Daube, *J. Vac. Sci. Technol. A* 5 (1987) 810.
- [27] J.M. Campbell, J. Nakamura, C.T. Campbell, *J. Catal.* 136 (1992) 24.

- [28] P.L.J. Gunter, J.W. Niemantsverdriet, F.H. Ribeiro, G.A. Somorjai, *Cat. Rev. – Sci. Eng.* 39 (1997) 77.
- [29] C.T. Campbell, *Surf. Sci. Rep.* 27 (1997) 1.
- [30] J.B. Park, J. Graciani, J. Evans, D. Stacchiola, S.D. Senanayake, L. Barrio, P. Liu, J.F. Sanz, J. Hrbek, J.A. Rodriguez, *J. Am. Chem. Soc.* 132 (2009) 356.
- [31] J.A. Rodriguez, J. Evans, J. Graciani, J.B. Park, P. Liu, J. Hrbek, J.F. Sanz, *J. Phys. Chem. C* 113 (2009) 7364.
- [32] J.A. Rodriguez, R. Liu, J. Hrbek, M. Perez, J. Evans, *J. Mol. Catal. A: Chem.* 281 (2008) 59.
- [33] J.A. Rodriguez, P. Liu, J. Hrbek, J. Evans, M. Perez, *Angew. Chem. Int. Ed.* 46 (2007) 1329.
- [34] J.A. Rodriguez, J. Graciani, J. Evans, J.B. Park, F. Yang, D. Stacchiola, S.D. Senanayake, S.G. Ma, M. Perez, P. Liu, J.F. Sanz, J. Hrbek, *Angew. Chem. – Int. Edit.* 48 (2009) 8047.
- [35] J.A. Rodriguez, P. Liu, X. Wang, W. Wen, J. Hanson, J. Hrbek, M. Perez, J. Evans, *Catal. Today* 143 (2009) 45.
- [36] D.W. Flaherty, N.T. Hahn, D. Ferrer, T.R. Engstrom, P.L. Tanaka, C.B. Mullins, *J. Phys. Chem. C* 113 (2009) 12742.
- [37] D.W. Flaherty, S.P. Berglund, C.B. Mullins, *J. Catal.* 269 (2010) 33.
- [38] G. Kresse, J. Hafner, *Phys. Rev. B* 47 (1993) 558.
- [39] G. Kresse, J. Hafner, *Phys. Rev. B* 49 (1994) 14251.
- [40] G. Kresse, J. Furthmuller, *Comput. Mater. Sci.* 6 (1996) 15.
- [41] G. Kresse, J. Furthmuller, *Phys. Rev. B* 54 (1996) 11169.
- [42] P.E. Blochl, *Phys. Rev. B* 50 (1994) 17953.
- [43] G. Kresse, D. Joubert, *Phys. Rev. B* 59 (1999) 1758.
- [44] P. Hohenberg, W. Kohn, *Phys. Rev.* 136 (1964) 864.
- [45] W. Kohn, L.J. Sham, *Phys. Rev.* 140 (1965) 1133.
- [46] J.P. Perdew, J.A. Chevary, S.H. Vosko, K.A. Jackson, M.R. Pederson, D.J. Singh, C. Fiolhais, *Phys. Rev. B* 46 (1992) 6671.
- [47] J.P. Perdew, Y. Wang, *Phys. Rev. B* 45 (1992) 13244.
- [48] J.P. Perdew, J.A. Chevary, S.H. Vosko, K.A. Jackson, M.R. Pederson, D.J. Singh, C. Fiolhais, *Phys. Rev. B* 48 (1993) 4978.
- [49] Y. Wang, S. Curtarolo, C. Jiang, R. Arroyave, T. Wang, G. Ceder, L.Q. Chen, Z.K. Liu, *Calphad* 28 (2004) 79.
- [50] G. Henkelman, H. Jonsson, *J. Chem. Phys.* 113 (2000) 9978.
- [51] G. Henkelman, B.P. Uberuaga, H. Jonsson, *J. Chem. Phys.* 113 (2000) 9901.
- [52] G. Henkelman, H. Jonsson, *J. Chem. Phys.* 111 (1999) 7010.
- [53] R.A. Olsen, G.J. Kroes, G. Henkelman, A. Arnaldsson, H. Jonsson, *J. Chem. Phys.* 121 (2004) 9776.
- [54] H.J. Monkhorst, J.D. Pack, *Phys. Rev. B* 13 (1976) 5188.
- [55] M. Methfessel, A.T. Paxton, *Phys. Rev. B* 40 (1989) 3616.
- [56] P.J. Feibelman, *Phys. Rev. B* 77 (2008) 165419.
- [57] J. Nakamura, J.M. Campbell, C.T. Campbell, *J. Chem. Soc., Faraday Trans.* 86 (1990) 2725.
- [58] H. Pines, W.O. Haag, *J. Am. Chem. Soc.* 82 (1960) 2471.
- [59] H. Kwart, *Acc. Chem. Res.* 15 (1982) 401.
- [60] F.H. Westheimer, *Chem. Rev.* 61 (1961) 265.
- [61] C.M. Kalamaras, P. Panagiotopoulou, D.I. Kondarides, A.M. Efstathiou, *J. Catal.* 264 (2009) 117.
- [62] F.C. Meunier, D. Tibiletti, A. Goguet, S. Shekhtman, C. Hardacre, R. Burch, *Catal. Today* 126 (2007) 143.
- [63] F.C. Meunier, G. Yablonsky, D. Reid, S.O. Shekhtman, C. Hardacre, R. Burch, M. Lazman, *Catal. Today* 138 (2008) 216.
- [64] O. Thinin, K. Rachedi, F. Diehl, P. Avenier, Y. Schuurman, *Top. Catal.* 52 (2009) 1940.
- [65] S. Haq, J. Harnett, A. Hodgson, *Surf. Sci.* 505 (2002) 171.
- [66] K.Y. Kung, P. Chen, F. Wei, Y.R. Shen, G.A. Somorjai, *Surf. Sci.* 463 (2000) L627.
- [67] G. Rupprechter, T. Dellwig, H. Unterhalt, H.-J. Freund, *J. Phys. Chem. B* 105 (2001) 3797.
- [68] G.A. Somorjai, *Introduction to Surface Chemistry and Catalysis*, John Wiley & Sons, Inc., New York, 1994.
- [69] M. Johansson, O. Lytken, I. Chorkendorff, *Surf. Sci.* 602 (2008) 1863.
- [70] M. Boudart, G. Djega-Mariadassou, *Kinetics of Heterogeneous Catalytic Reactions*, Princeton University Press, Princeton, NJ, 1984.
- [71] K. McCrea, J.S. Parker, P. Chen, G. Somorjai, *Surf. Sci.* 494 (2001) 238.
- [72] X. Su, P.S. Cremer, Y.R. Shen, G.A. Somorjai, *J. Am. Chem. Soc.* 119 (1997) 3994.
- [73] R.J. Madon, D. Braden, S. Kandoi, P. Nagel, M. Mavrikakis, J.A. Dumesic, *J. Catal.* 281 (2011) 1.
- [74] N. Guo, B.R. Fingland, W.D. Williams, V.F. Kispersky, J. Jelic, W.N. Delgass, F.H. Ribeiro, R.J. Meyer, J.T. Miller, *PCCP* 12 (2010) 5678.
- [75] G.B. Fisher, B.A. Sexton, *Phys. Rev. Lett.* 44 (1980) 683.
- [76] T.W. Haas, J.T. Grant, G.J. Dooley, *J. Appl. Phys.* 43 (1972) 1853.
- [77] T.A. Land, T. Michely, R.J. Behm, J.C. Hemminger, G. Comsa, *J. Chem. Phys.* 97 (1992) 6774.
- [78] V. Johaneck, A.B. De la Ree, J.C. Hemminger, *J. Phys. Chem. C* 113 (2009) 4441.
- [79] Y.L. Tsai, C. Xu, B.E. Koel, *Surf. Sci.* 385 (1997) 37.
- [80] D. Tibiletti, F.C. Meunier, A. Goguet, D. Reid, R. Burch, M. Boaro, M. Vicario, A. Trovarelli, *J. Catal.* 244 (2006) 183.
- [81] M.R. Columbia, A.M. Crabtree, P.A. Thiel, *J. Am. Chem. Soc.* 114 (1992) 1231.
- [82] N.R. Avery, *Appl. Surf. Sci.* 11–12 (1982) 774.
- [83] N. Schumacher, K. Andersson, L.C. Grabow, M. Mavrikakis, J. Nerlov, I. Chorkendorff, *Surf. Sci.* 602 (2008) 702.
- [84] H. Chen, W. Zhu, Z. Zhang, *Phys. Rev. Lett.* 104 (2010) 186101.
- [85] J. Kugai, J.T. Miller, N. Guo, C. Song, *J. Catal.* 277 (2011) 46.